48th AIAA Aerospace Sciences Meeting Including the New Horizons Forum and Aerospace Exposition
4 - 7 January 2010, Orlando, Florida
AIAA 2010-996

Incorporating Irregular Nonlinear Waves in Coupled Simulation of Offshore Wind Turbines

Puneet Agarwal*
Stress Engineering Services, Houston, TX 77041
Lance Manuel†
Department of Civil, Architectural, and Environmental Engineering
The University of Texas, Austin, TX 78712

Design of an offshore wind turbine requires estimation of loads on its rotor, tower and supporting structure. These loads are obtained by time-domain simulations of the coupled aero-servo-hydro-elastic model of the wind turbine. Accuracy of predicted loads depends on assumptions made in the simulation models employed, both for the turbine and for the input wind and wave conditions. Currently, waves are simulated using a linear irregular wave theory, which is not appropriate for nonlinear waves in shallow water depths, where wind farms are typically sited. The present study investigates the use of irregular nonlinear (second-order) waves for estimating loads on the support structure (monopile) of an offshore wind turbine. We present the theory for the irregular nonlinear model and incorporate it in the commonly used wind turbine simulation software, FAST, which had been developed by National Renewable Energy Laboratory (NREL), but which had the modeling capability only for irregular linear waves. We use an efficient algorithm for computation of nonlinear wave elevation and kinematics, so that a large number of time-domain simulations, which are required for prediction of long-term loads using statistical extrapolation, can easily be performed. To illustrate the influence of the alternative wave models, we compute loads at the base of the monopile of the NREL 5MW baseline wind turbine model using linear and nonlinear irregular wave models. We show that for a given environmental condition (i.e., the mean wind speed and the significant wave height), extreme loads are larger when computed using the nonlinear wave model. We then compute long-term loads, which are required for a design load case according to the International Electrotechnical Commission guidelines. We show that 20-year long-term loads can be significantly higher when the nonlinear wave model is used.

I. Introduction

Offshore wind energy is becoming an important part of the overall energy mix in Europe and has great potential within the United States and other parts of the world. The potential for offshore wind power in the United States, in water depths less than 30 meters where current fixed-bottom support structure technologies can be used, is about 98 GW.[1] Europe has a target of generating about 12% of its electricity from wind by the year 2020, of which about one-third, or about 30 GW (gigawatts), is expected to come from offshore projects.[2,3] To meet such demand, it is important to develop appropriate simulation tools for design of offshore wind turbines.

Response of an offshore wind turbine to the input wind and waves, both of which are stochastic in nature, is estimated using coupled aero-servo-hydro-elastic simulation in time domain. Such time-domain simulations are also used to obtain the data on load extremes, which are needed for calculation of long-term (for a return period of 20 or 50 years) extreme loads using the statistical extrapolation method as recommended by the IEC 61400-3 standard[4] from International Electrotechnical Commission (IEC). The accuracy of the turbine response depends on the proper modeling and interfacing of various parts of the physics (aeroelasticity,

*Senior Analyst
†Associate Professor

dynamics, control systems etc) of an offshore wind turbine, as well as on the appropriate modeling of the incident wind and waves. In this paper, we exclusively focus on how alternate wave models influence the turbine response.

The current practice to model waves on offshore wind turbines is limited to linear irregular waves, which are not an accurate representation of waves in shallow waters where offshore wind turbines are most commonly sited. In shallow waters, waves are generally nonlinear in nature, therefore we attempt to incorporate a nonlinear irregular wave model in the coupled aero-servo-hydro-elastic simulation of offshore wind turbines.

Among several nonlinear irregular wave models available in the literature, the one that has been recommended by offshore guidelines[5] and that has been increasingly applied to a variety of problems in recent years[5–8] is the second-order nonlinear irregular wave model developed by Sharma and Dean[9] for finite water depths. This second-order nonlinear irregular wave model is based on the solution of the Laplace equation in velocity potential, associated with nonlinear boundary conditions, using a second-order perturbation expansion of the relevant variables (velocity potential and sea surface elevation) and a Taylor series expansion of nonlinear boundary conditions about the free surface. Such an approach was first presented by Longuet-Higgins[10] and Hasselmann[11] for infinite water depths. Since its introduction in 1979, the second-order nonlinear irregular wave model developed by Sharma and Dean has been studied by several researchers. Hu and Zhao,[12] Langley,[13] Longuet-Higgins[14] and Forristall,[15] among others, investigated the statistical properties (skewness in particular) of this nonlinear irregular wave model. Forristall[16] compared various stretching techniques for calculating wave kinematics above the mean sea level. Due to such maturity of this nonlinear irregular wave model and because of its theoretical basis (as distinct from some semi-empirical models, such as the New Wave model,[17] the constrained New Wave model[18] and a hybrid wave model[19]), and also due to its computational efficiency for simulations (as distinct from more realistic though computationally very expensive models based on Boussinesq theory[20,21]), we will use this second-order nonlinear irregular wave model, as developed by Sharma and Dean,[9] to simulate nonlinear irregular waves in shallow water depths for offshore wind turbine loads predictions.

The outline of this paper is as follows: we first present an overview of the hydrodynamics—employing the currently used linear irregular wave model—in the coupled simulation of offshore wind turbines. We present the theoretical formulation of the second-order nonlinear irregular wave model. We limit our focus to unidirectional (long-crested) waves. We then present a detailed procedure, which we have incorporated in the turbine response simulation software, FAST,[22] for efficient simulation of the sea surface elevation and the water particle kinematics process based on the nonlinear irregular wave model. We use a utility-scale 5MW offshore wind turbine model developed at the National Renewable Energy Laboratory (NREL)[23] to compare turbine response (mainly the fore-aft tower bending moment at the mudline) due to linear and nonlinear irregular waves. we compute the turbine response for a representative environmental state, and show that when nonlinear waves are used, turbine loads can be larger and tower dynamics can be influenced to some extent as well. We finally show that long-term loads are significantly larger with nonlinear waves, and therefore, it is important to use nonlinear wave model in the design of offshore wind turbines.

II. Hydrodynamics in Coupled Simulation of Offshore Wind Turbines

Structural response of wind turbines—both onshore and offshore—in the time domain is analyzed using coupled aero-servo-hydro-elastic simulation programs. One such program is FAST (Fatigue, Aerodynamics, Structures and Turbulence),[22] developed at the National Renewable Energy Laboratory (NREL). FAST is a medium-complexity program that models a wind turbine as a combination of rigid and flexible bodies wherein flexible beam elements (representing the blades and the tower) are formulated in terms of generalized coordinates. Aerodynamic forces on the rotating blades of a horizontal-axis wind turbine are commonly computed using the blade element momentum theory.[24] FAST models various control systems including blade and pitch control, yaw control, and high-speed shaft brake control. FAST uses irregular linear wave model with Morison's equation to compute hydrodynamic loads for offshore wind turbines. Perhaps the most important aspect of the FAST program is the proper interfacing of various parts of the physics—aeroelasticity, dynamics, control systems, hydrodymaics, etc—of an offshore wind turbine. Without such coupling, it is not possible to accurately assess the response of wind turbines. We next discuss hydrodynamic calculations in FAST, while highlighting its limitations to model shallow water waves.

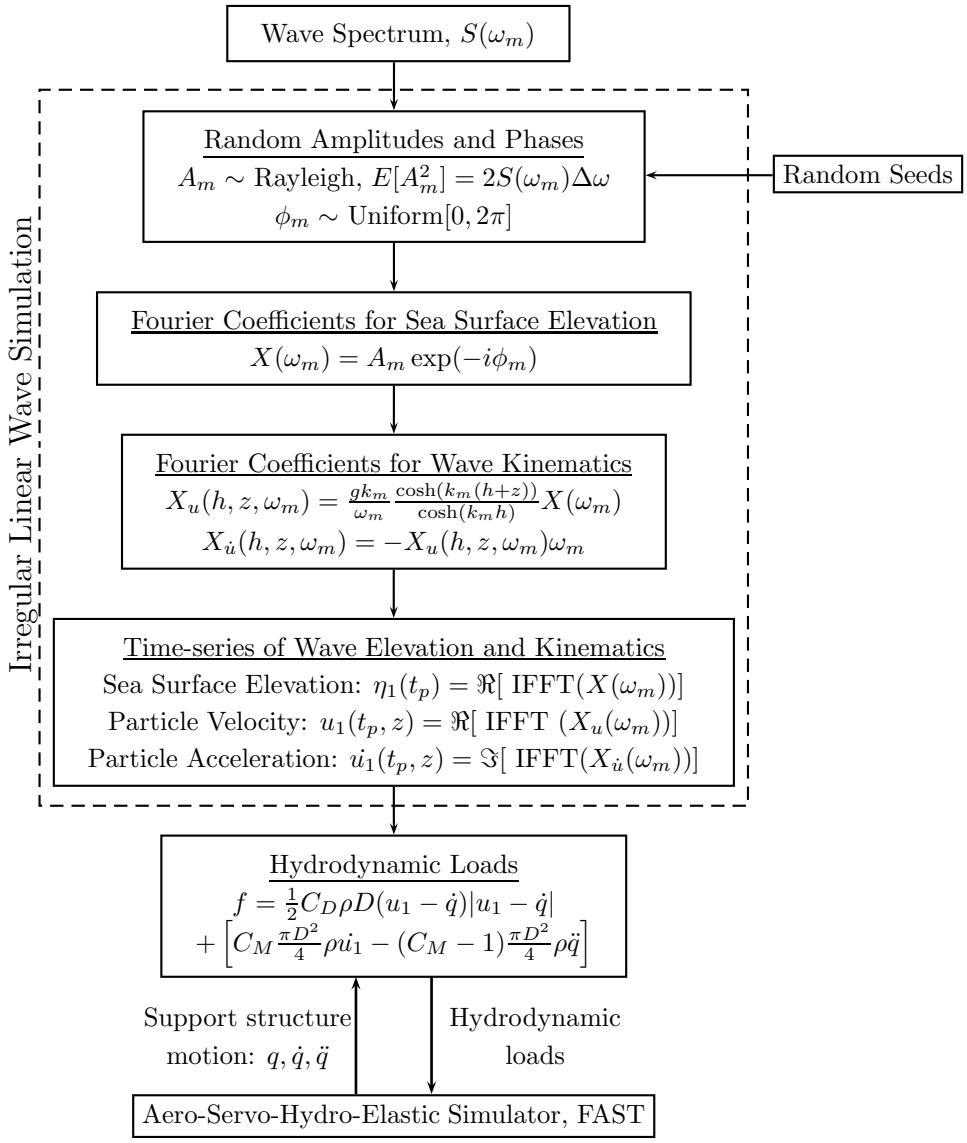

Figure 1. Flow-chart for Calculation of Irregular Linear Wave Kinematics and Hydrodynamic Loads on the Monopile Support Structure in FAST.

II.A. Irregular Linear Wave Simulation

In the current version of FAST program, waves are modeled using the irregular linear wave model, which is the most common model to represent stochastic (or irregular) ocean waves. A flow-chart for calculation of wave kinematics using irregular linear wave model for unidirectional waves and the resulting hydrodynamic loads on the monopile support structure of the offshore wind turbine is shown in Fig. 1. These calculations are rather standard and may be found in several well-established references,[25,26] so we discuss them only briefly here.

The starting point in simulation of irregular waves is a (one-sided) wave spectrum, $S(\omega_m)$, where ω_m refers to the frequency of the m^{th} wave component; the integer, m, refers to a frequency index that ranges from 1 to N. Random seeds are used to generate the random phase, ϕ_m, which are assumed to be uniformly distributed over $[0, 2\pi]$, and Rayleigh distributed amplitudes, A_m, whose mean square value, $E[A_m^2]$, is $2S(\omega_m)\Delta\omega$. Fourier coefficients, $X(\omega_m)$, for the the sea surface elevation process, $\eta_1(x, t_p)$, (the subscript "1" denotes the linear, or first-order, wave model) are then computed. Here, the spatial location is denoted

by x (see Fig. 2 for a schematic), and the time-instant is denoted by $t_p = p\Delta t$, where $\Delta t = T/N$, such that $p = 1, 2, ..., N$. Fourier coefficients for the water particle velocity, $X_u(h, z, \omega_m)$, and for the water particle acceleration, $X_{\dot{u}}(h, z, \omega_m)$, are then computed using formulae from irregular linear wave model as shown in the flow-chart. Once these are available, time-series of sea surface elevation, and water particle velocity and acceleration, are computed using the inverse Fast Fourier Transform (IFFT) algorithm. Hydrodynamic forces per unit length, $f(0, z, t)$ (for simplicity of notation, we will drop the argument $(0, z, t)$ hereon), at any node located at a depth z, along the centerline of the monopile, which we arbitrarily chose at $x = 0$ (Fig. 2) are computed using the Morison's equation[25] as follows:

$$f = f_D + f_M = \frac{1}{2} C_D \rho D (u - \dot{q})|u - \dot{q}| + \left[C_M \frac{\pi D^2}{4} \rho \dot{u} - (C_M - 1) \frac{\pi D^2}{4} \rho \ddot{q} \right] \tag{1}$$

where f_D and f_M are drag and inertia forces, respectively. Also, C_D and C_M are the drag and the inertia coefficients, respectively; ρ is the density of water, and D is the diameter of the cylinder. The variables $u(= u_1)$ and $\dot{u}(= \dot{u}_1)$ are the undisturbed water particle velocity and acceleration, respectively. Variables $\dot{q}$ and $\ddot{q}$ denote the velocity and acceleration of the corresponding node on the structure, which are obtained from the dynamic analysis of the entire turbine system, including blade aero-elasticity, structural dynamics, control actions, generator etc at each time step. Note that such aero-servo-elastic analysis needs to be "coupled" with the hydrodynamic analysis in order to correctly account for the relative motion between water particles and the monopile in calculation of hydrodynamic loads according to Eq. 1.

One limitation of the existing FAST program is the use of linear irregular wave model, which is not appropriate for shallow water depths, where waves are irregular as well as nonlinear. We address this model limitation by incorporating a second-order nonlinear irregular wave model in FAST program for the coupled aero-servo-hydro-elastic simulation of offshore wind turbines.

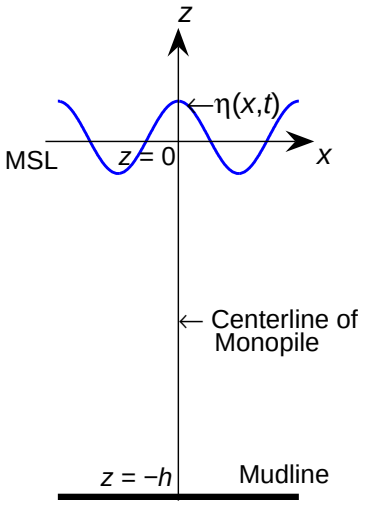

Figure 2. Schematic illustrating the spatial coordinate, x, the vertical coordinate, z, and the sea surface elevation, $\eta(x, t)$, relative to the mean sea level (MSL).

III. Second-order Nonlinear Irregular Waves

Linear wave theory for regular or irregular waves involves solution of Laplace's equation expressed in terms of a velocity potential and the use of linearized boundary conditions.[25] For nonlinear waves, the theory involves application of a perturbation approach to solve Laplace's equation with nonlinear boundary conditions. Sharma and Dean[9] used such an approach to derive a nonlinear wave theory for finite water depths. We will use the formulation of Sharma and Dean, which is described very briefly below. This theory is also recommended in some guidelines for offshore structures.[5,8]

III.A. Theoretical Model

The nonlinear sea surface elevation, $\eta(t)$, may be expressed as a sum of first- and second-order components, such that $\eta(t) = \eta_1(t) + \eta_2(t)$. The first-order component, $\eta_1(t)$, is expressed as in linear wave theory by

$$\eta_1(t) = \sum_{m=1}^{N} A_m \cos(\omega_m t - \phi_m) \tag{2}$$

where ω_m refers to the frequency of the m^{th} wave component. The random phase, ϕ_m, and the amplitudes of the wave components, A_m, have been defined in Fig. 1.

The second-order component, $\eta_2(t)$, is obtained as a result of the interactions of sums and differences of frequencies as follows:

$$\eta_2(t) = \sum_{m=1}^{N} \sum_{n=1}^{N} \left[A_m A_n \left\{ B^-_{mn} \cos(\psi_m - \psi_n) + B^+_{mn} \cos(\psi_m + \psi_n) \right\} \right] \tag{3}$$

where $\psi_m = (\omega_m t - \phi_m)$ and the second-order transfer functions, B^-_{mn} and B^+_{mn}, are obtained from solution of Laplace's equation for the velocity potential with nonlinear boundary conditions. They (i.e., B^-_{mn} and B^+_{mn}) are functions of frequency and wave number and are independent of the spectrum used.

The velocity potential, Φ, is comprised of first and second-order components such that $\Phi = \Phi_1 + \Phi_2$. These first and second-order velocity potentials are given as follows:

$$\Phi_1 = \sum_{m=1}^{N} b_m \frac{\cosh(k_m(h+z))}{\cosh(k_m h)} \sin\psi_m \tag{4}$$

$$\Phi_2 = \frac{1}{4} \sum_{m=1}^{N} \sum_{n=1}^{N} \left[b_m b_n \frac{\cosh(k^{\pm}_{mn}(h+z))}{\cosh(k^{\pm}_{mn} h)} \frac{D^{\pm}_{mn}}{(\omega_m \pm \omega_n)} \sin(\psi_m \pm \psi_n) \right] \tag{5}$$

where $b_m = A_m g/\omega_m$ and $k^{\pm}_{mn} = |k_m \pm k_n|$. Also, the linear dispersion relation, $\omega_m^2 = g k_m \tanh(k_m h)$, relates the wave number, k_m, to the frequency, ω_m, where h is the water depth and g is acceleration due to gravity. Expressions for the transfer functions, $B^{\pm}_{mn}$ and $D^{\pm}_{mn}$, appearing in Eqs. 3 and 5, respectively, were derived by Sharma and Dean,[9] and are also summarized in Appendix A. The horizontal water particle velocity, $u(z,t)$, and the horizontal water particle acceleration $\dot{u}(z,t)$ may be obtained from the velocity potential by taking derivatives such that

$$u(z,t) = \partial\Phi/\partial x, \dot{u}(z,t) = \partial u(z,t)/\partial t \tag{6}$$

Second-order waves are thus obtained as a result of sum and difference interactions between pairs of frequencies. The phases of the second-order contributions are also determined by sum and difference interactions of the phases of the first-order component phases, which are random.

III.A.1. Statistics of Nonlinear Sea Surface Elevation

The area under the power spectral density function of the sea surface elevation process, $S(\omega_m)$, is equal to the variance of a simulated linear irregular sea surface elevation ensemble, a fact that can be used to evaluate the accuracy of the simulations. Likewise, one can compute the skewness from wave spectra that should match that from a simulated nonlinear sea surface elevation ensemble. In fact, nonlinearity described by the second-order irregular wave model is directly related to the process skewness. Langley[13] developed a procedure, based on Volterra series models, to compute the statistical moments of a nonlinear sea surface elevation process. The procedure for calculation of variance, skewness and kurtosis from spectrum is not presented here for brevity, and the reader is referred to the paper by Langley.[13]

III.A.2. Validity of the Second-order Wave Model

While the second-order irregular wave model is a more accurate representation of irregular seas in shallow waters compared to the linear irregular wave model, it obviously does not model the complete nonlinear character of waves, and is not valid for all cases. The physical parameter that determines the range of validity is the wave steepness. When the wave steepness exceeds a certain value, the second-order model is no longer valid, and a higher-order model is required. In fact, when waves become too steep, they can break and no model based on solution of Laplace's equation (in terms of velocity potential) is valid. The wave steepness, s, according to DNV guidelines,[5] is defined $s = H_s/L_z$, where H_s is the significant wave height and L_z is the wavelength based on the mean zero-crossing period (obtained using the linear dispersion relation). Based on results from numerical simulations, Hu and Zhao[12] suggested that the second-order wave model presented above is valid as long as the wave steepness is smaller than approximately 0.08. This empirical limit can be used to ascertain whether the second-order wave model should be used for a given significant wave height and wavelength combination.

III.B. Numerical Implementation

While this second-order wave model has been discussed in several published studies,[5,15,27–29] a complete recipe for the numerical simulation of such second-order waves is not yet available in one place. This is in contrast to the case for linear irregular waves, for which a recipe for numerical simulation with all the

pertinent details is available in several places.[25,30] Therefore, we discuss the numerical simulation of second-order waves in detail below.

Numerical Simulation of irregular (random) linear or first-order waves, which involves a single summation (Eq. 2), can be efficiently performed using the Inverse Fast Fourier Transform (IFFT). On the other hand, simulation of random nonlinear or second-order waves according to Eq. 3 involves a double summation, which can be very expensive. However, one can rewrite the double summation as a single summation by appropriately re-assembling and rewriting indices (or coefficients) in the double summation. Once the indices for an equivalent single summation are assembled, a one-dimensional IFFT procedure, similar to that for linear waves, can be used to perform the nonlinear wave simulations more efficiently.

The double sum in Eq. 3, to simulate the second-order component of the sea surface elevation process, may be rewritten as

$$\eta_2(t_p) = \Re\left[\sum_{m=1}^{N}\sum_{n=1}^{N}\left[X_{mn}^{\pm}\exp\left(-i(m\pm n)\Delta\omega p\Delta t\right)\right]\right] \tag{7}$$

$$X_{mn}^{\pm} = A_m A_n B_{mn}^{\pm}\exp(-i(\phi_m \pm \phi_n)) \tag{8}$$

where $t_p = p\Delta t$, $\omega_m = m\Delta\omega$ and $\omega_n = n\Delta\omega$; $m, n, p = 1, 2, ..., N$. Also, $\Delta t = T/N$, where T is the period (duration) of the simulations and $\Delta\omega = 2\pi/T$.

Performing this sum (as given by Eq. 7) is computationally inefficient even for moderate values of N, as a total of N^2 terms are to be summed. Therefore, we seek an implementation based on the IFFT (inverse Fast Fourier Transform) technique. We start by rewriting the double summation in Eq. 7 as an equivalent single summation as follows:

$$\eta_2(t_p) = \Re\left[\sum_{j=1}^{N} Y_j^{\pm}\exp\left(-i\frac{2\pi j}{N}p\right)\right] \tag{9}$$

Note that the term within the summation in Eq. 9 is the definition of the inverse discrete Fourier transform of $Y_j^{\pm}$, which can be efficiently computed using inverse Fast Fourier transform (IFFT) techniques, such that

$$\eta_2(t_p) = \Re\left[IFFT\left(Y_j^{\pm}\right)\right]. \tag{10}$$

The Fourier coefficients $Y_j^{\pm}$ are obtained by "equating" Eq. 9 to Eq. 7. This involves conversion of a two-dimensional sum over N^2 terms to a one-dimensional sum over N terms by collecting all (m, n) pairs that yield a sum, or difference, equal to j, for sum- and difference-frequency interactions, respectively. For example, $(m, n) = (1, 3), (2, 2)$ and $(3, 1)$ would all yield a sum for $j = 4$; so, these three X_{mn}^{+} contributions must be collected to form Y_4^{+}. Note that both the time index, p, and the frequency indices, j, still range from 1 to N.

For sum-frequency interaction, as m and n range from 1 to M, the sum, $(m + n)$, ranges from 2 to $2M$. Note that more than one (m, n) pair may result in the sum, $j = m + n$. The Fourier coefficients Y_j^{+}, for $2 \le j \le 2M$ are obtained as

$$Y_j^{+} = \underbrace{\sum\sum}_{m+n=j} X_{mn}^{+} \tag{11}$$

with $Y_1^{+} = 0$.

For difference-frequency interactions, as m and n range from 1 to M, the difference, $(m-n)$, ranges from $-(M-1)$ to $(M-1)$. Note that Eq. 7 requires only cosine terms to be computed, and since $\cos(\psi_m - \psi_n)$ $= \cos(-(\psi_m - \psi_n))$, negative difference-frequencies have the same effect as positive difference-frequencies. Therefore, we need to concern ourselves only with $\cos(|\psi_m - \psi_n|)$ or, effectively, with $|m-n|$. When creating the terms Y_j^{-}, we need to keep the consistent phases, ϕ_{mn}^{-} $(= \phi_m - \phi_n)$, to make sure the IFFT-based simulation (Eq. 9) is the same as the summation-based simulation (Eq. 7). Following from the symmetry of the cosine function, we need

$$\phi_{mn}^{-} = \begin{cases} (\phi_m - \phi_n), & m > n \\ -(\phi_m - \phi_n), & m \le n \end{cases} \tag{12}$$

The Fourier coefficients Y_j^- for $1 \le j \le (M-1)$ are obtained as

$$Y_j^- = \underbrace{\sum\sum}_{|m-n|=j} X_{mn}^- \tag{13}$$

with $Y_j^- = 0$ for $j \ge M$.

Using the procedure described above, we can obtain the coefficients, $Y_j^\pm$, for Eq. 9 from Eqs. 11 and 13, and simulate the time series of the second-order sea surface elevation, $\eta_2(t_p)$, using Eq. 10.

Second-order components of the wave kinematics, such as the horizontal particle velocity at $x = 0$ and at a depth z, $u(0, z, t_p)$, and the horizontal particle acceleration, $\dot{u}(0, z, t_p)$, can be simulated by a similar approach. Again, to simplify notation, we denote these variables as $u(z, t_p)$ and $\dot{u}(z, t_p)$. By substituting the second-order velocity potential (Eq. 5) in the definition of particle kinematics given by Eqs. 6, we obtain the following expressions for velocity and acceleration:

$$u_2(z,t_p) = \Re\left[\sum_{m=1}^{N}\sum_{n=1}^{N}\left[U_{mn}^\pm \exp\left(-i(m\pm n)\frac{2\pi}{N}p\right)\right]\right] \tag{14}$$

$$\dot{u}_2(z,t_p) = \Im\left[\sum_{m=1}^{N}\sum_{n=1}^{N}\left[\dot{U}_{mn}^\pm \exp\left(-i(m\pm n)\frac{2\pi}{N}p\right)\right]\right] \tag{15}$$

where $\Im(\cdot)$ denotes the imaginary component of the argument, and

$$U_{mn}^\pm = Z_{mn}^\pm \exp(-i(\phi_m \pm \phi_n) sgn(m \pm n)) \tag{16}$$

$$\dot{U}_{mn}^\pm = -(\omega_m \pm \omega_n) U_{mn}^\pm \tag{17}$$

$$Z_{mn}^\pm = \frac{1}{4} b_m b_n \frac{\cosh(k_{mn}^\pm (h+z))}{\cosh(k_{mn}^\pm h)} \frac{D_{mn}^\pm}{(\omega_m \pm \omega_n)} k_{mn}^\pm \tag{18}$$

Also, $sgn(q)$ denotes the signum function such that

$$sgn(q) = \begin{cases} -1 & if\ q < 0 \\ 0 & if\ q = 0 \\ 1 & if\ q > 0 \end{cases} \tag{19}$$

The simulation of particle velocity and acceleration according to Eqs. 14 and 15, respectively, requires a double summation. We can reduce these double summations to single summations just as we did for sea surface elevation, and can readily simulate particle velocity and acceleration according to the following equations:

$$u_2(z,t_p) = \Re\left[IFFT\left(W_j^\pm\right)\right] \tag{20}$$

$$\dot{u}_2(z,t_p) = \Im\left[IFFT\left(\dot{W}_j^\pm\right)\right] \tag{21}$$

The Fourier coefficients, $W_j^\pm$, in Eq. 20 and $\dot{W}_j^\pm$ in Eq. 21, are assembled from the coefficients, $U_{mn}^\pm$ and $\dot{U}_{mn}^\pm$, respectively, using exactly the same approach as for the coefficients, $Y_j^\pm$, in Eq. 9 that were in turn assembled from the coefficients, $X_{mn}^\pm$, in Eq. 7.

A flowchart for calculation of irregular nonlinear wave kinematics and resulting hydrodynamic loads is described in Fig. 3. These calculations are implemented in the computer program FAST for coupled aero-servo-hydro-elastic analysis of offshore wind turbines. A switch for irregular wave model (linear or nonlinear) is the only additional input to be provided by the user. Because of the use of the efficient simulation algorithm described above, the computation time for nonlinear irregular model is similar to that for the linear irregular waves, and a large number of time-domain simulations required for load extrapolation can easily be performed.

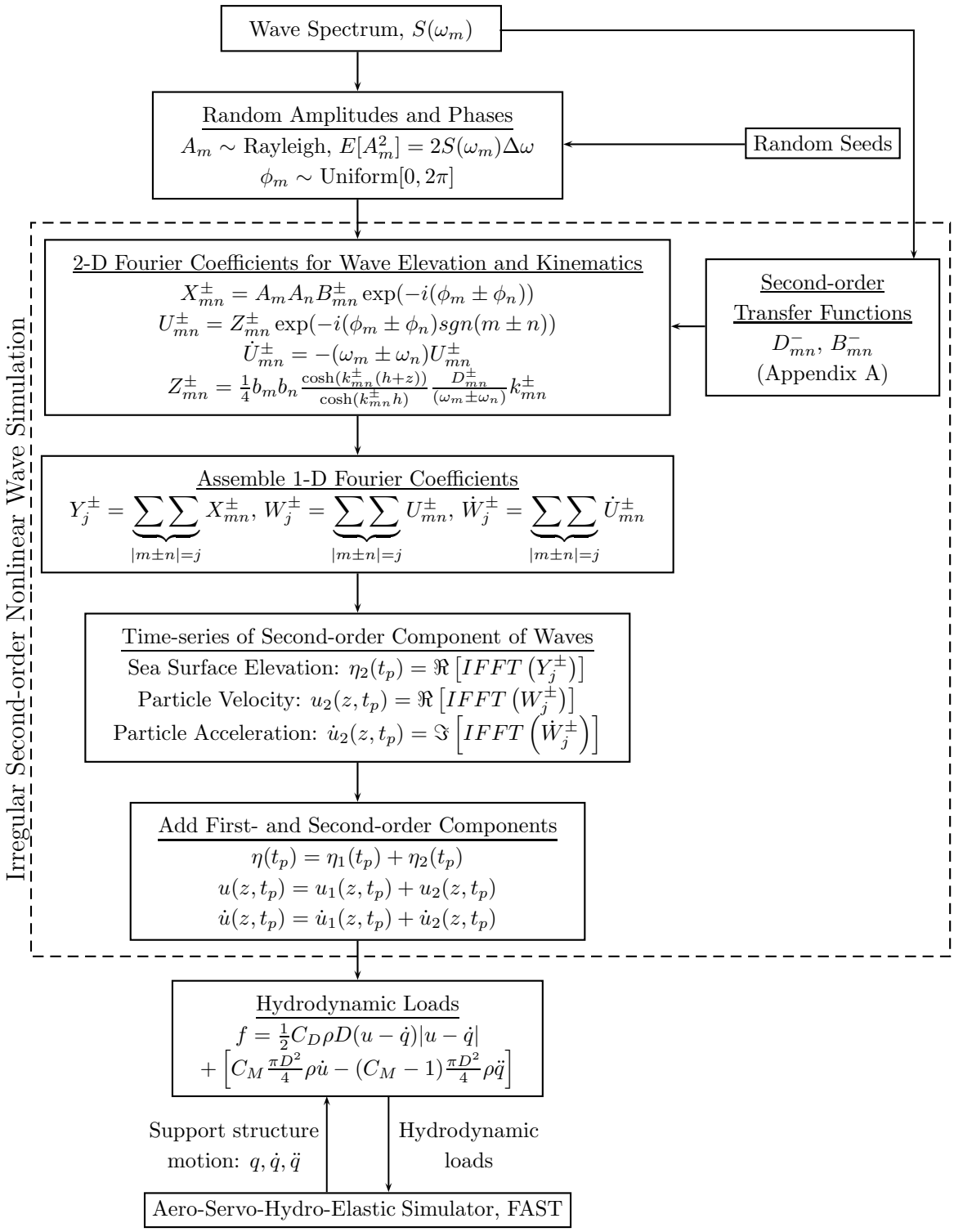

Figure 3. Flow-chart for Calculation of Second-order Nonlinear Irregular Wave Kinematics and Hydrodynamic Loads on the Monopile Support Structure in FAST.

Table 1. Comparison of statistics of the sea surface elevation process simulated using linear and nonlinear irregular wave models for a JONSWAP spectrum with H_s = 7.5 m and T_p = 12.3 sec.

Sea-surface elevation statistics	Wave model	
	linear	nonlinear
Std.Dev. (m)	1.8	2.0
Max (m)	5.6	6.6
Skewness	0.0	0.1
Kurtosis	2.9	3.2
Peak Factor*	3.0	3.3

* Ten-minute median extreme peak factor (computed based on 50 simulations).

III.C. Wave Simulation Example

We simulate linear and nonlinear waves with significant wave height, H_s, of 7.5 m. We assume a peak spectral period, T_p, of 12.3 sec, and use a JONSWAP spectrum. A water depth of 20 m is assumed (same as for the wind turbine model discussed later in the paper). Based on 50 simulations, each of 10-minute duration, average value of statistical moments, maxima and extreme peak factors for the sea surface elevation process, simulated using linear and nonlinear irregular waves, are summarized in Table 1. Statistical moments are computed from the simulated time series, and they were found to match the target moments computed from a theoretical formulation presented by Langley.[13] Nonlinear waves have a non-zero skewness and a kurtosis larger than three, which indicates the non-Gaussian character of these nonlinear waves. Because of the larger skewness and kurtosis and, hence the somewhat larger peak factor, associated with nonlinear waves, extremes based on the use of a nonlinear wave theory are larger than those based on linear waves. Since nonlinear waves tend to have sharper crests, the maximum of the sea surface elevation is larger (by about 1 m or 18%) than is the case for linear waves.

Estimates of the maximum horizontal particle velocity, u_{max}, and acceleration, $\dot{u}_{max}$, at the free surface are presented in Table 2. It is clearly seen that maximum velocity and acceleration values increase when nonlinear waves are modeled, and the increase is about 40% for the water depth of 20 m. Table 2 also shows that influence of nonlinear waves decreases with increase in water depth. This is because at larger water depths, waves tend to become more and more linear.

As a result of larger particle velocities and accelerations, the hydrodynamic loads, and hence the lateral base forces, on a monopile would be larger for nonlinear waves, compared to those for linear waves. Furthermore, due to larger wave heights for nonlinear waves, it is expected that a greater portion of the monopile would get submerged and, as a result, the loads would be further amplified. For a more detailed discussion of influence of nonlinear waves on drag and inertia forces, and how forces vary for a range of monopile diameter and water depths, the reader is referred to a previous study by authors.[31]

Table 2. Comparison of maximum water particle velocity, u_{max}, acceleration, $\dot{u}_{max}$, at the free surface, averaged over fifty simulations, computed with linear and nonlinear irregular waves using a JONSWAP spectrum with H_s = 7.5 m and T_p = 12.3 sec.

	Depth = 20 m		Depth = 30 m	
	u_{max} (m/s)	$\dot{u}_{max}$ (m/s^2)	u_{max} (m/s)	$\dot{u}_{max}$ (m/s^2)
Linear Waves	5.05	3.64	4.59	3.81
Nonlinear Waves	7.05	5.20	5.38	4.10
Ratio	1.40	1.43	1.17	1.08

IV. Effect of Wave Model on Turbine Loads

We now investigate how the alternative wave models discussed above affect the response of an offshore wind turbine. We focus on the fore-aft tower bending moment and the shear force at mudline, as these are directly effected by waves. Loads on the turbine rotor, on the other hand, are not affected as much by waves as by wind. In the following, we first discuss the turbine model used, and then compare time-series and statistics of the fore-aft tower bending moment resulting from linear and nonlinear wave models. We finally compute loads for a return period of 20 years in order to assess influence of the alternative wave models on long-term loads.

IV.A. Turbine Model

A 5MW wind turbine model developed at NREL[23] closely representing utility-scale offshore wind turbines being manufactured today is considered here. The turbine is a variable-speed, collective pitch-controlled machine with a maximum rotor speed of 12.1 rpm; its rated wind speed is 11.5 m/s. It is assumed to have a hub height of 90 meters above the mean sea level, and a rotor diameter of 126 meters. It is assumed to be sited in 20 meters of water; it has a monopile support structure of 6 m diameter, which is assumed to be rigidly connected to the seafloor. The turbine is assumed to be installed at an IEC Class I-B wind regime site.[4] A Kaimal power spectrum and an exponential coherence spectrum are employed to describe the inflow turbulence random field over the rotor plane, which is simulated using the computer program, TurbSim.[32]

For the hydrodynamic loading on the support structure, irregular long-crested waves are simulated using a JONSWAP spectrum.[33] This same wave spectrum is used for simulating linear and nonlinear irregular waves. Hydrodynamic loads are computed using Morison's equation (Eq. 1); Wheeler stretching[5] is used to represent water particle kinematics and hydrodynamic loads up to the changing instantaneous sea surface.

IV.B. Turbine Response

We consider environmental conditions involving a significant wave height of 7.5 m with a mean wind speed of 18 m/s. This combination of V and H_s governs long-term fore-aft tower bending moment at the mudline for a return period of 20 years; we will discuss long-term loads later in the paper, and for now, we discuss how linear and nonlinear irregular waves influence the turbine response.

Table 3 shows statistics of the fore-aft tower base shear (FATBS) and the fore-aft tower bending moment (FATBM) at the mudline, averaged over 100 ten-minute simulations. The 10-minute maximum FATBM with the nonlinear waves is 99 MN-m, which is about 9% larger than that due to the linear waves. The maximum FATBS due to the nonlinear waves is, however, almost 27% larger than that due to the linear waves. Note that because of a larger lever arm (hub height of 90 meters), aerodynamic forces on the turbine rotor have a greater influence on the fore-aft tower bending moment than they have on the fore-aft tower base shear (see[34] for more details on how wave nonlinearity affects tower loads in presence and absence of wind). Shear forces at the base of the tower are influenced more directly by hydrodynamic loads, hence the larger sea surface elevation and particle kinematics due to nonlinear waves result in a greater increase in base shear than in bending moment.

Table 3. Comparison of 10-minute statistics, averaged over 100 simulations, of the fore-aft tower base shear (FATBS) and the fore-aft tower bending moment (FATBM) at the mudline for linear and nonlinear waves, for a JONSWAP spectrum with H_s = 7.5 m and T_p = 12.3 sec, and wind speed, V = 18 m/s.

	FATBS (MN)		FATBM (MN-m)	
Wave Model →	linear	nonlinear	linear	nonlinear
Max	3.06	3.88	90.43	98.58
Std.Dev.	0.81	0.86	13.43	14.04
Skewness	0.08	0.25	0.15	0.22
Kurtosis	3.04	3.81	3.23	3.60
Peak Factor	3.32	4.08	3.70	4.10

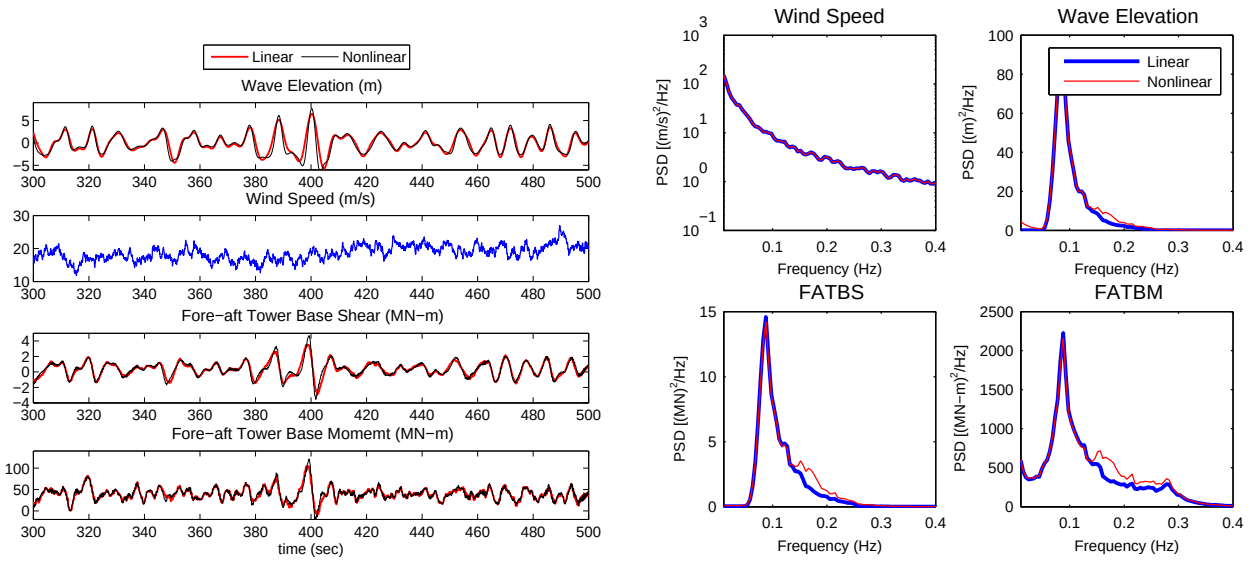

(a) A 200-second segment of time series

(b) Power spectral densities (PSD)

Figure 4. (a) Time series and (b) power spectral densities of the wave elevation, wind speed, fore-aft tower base shear (FATBS) and for-aft tower bending moment (FATBM) at mudline for V = 18 m/s, H_s = 7.5 m (T_p = 12.3 sec).

We can further understand hydrodynamic loads by studying the non-Gaussian character in these load processes. The degree to which a process is non-Gaussian relates to the extent by which its skewness deviates from zero and its kurtosis deviates from three. A process with a positive skewness and a kurtosis greater than three (as is the case here) will generally lead to larger peak factors. This will, in turn, result in larger extremes associated with any specified rare probability level compared to those predicted for a Gaussian process. Note that it is such low exceedance probability levels that are of eventual interest in predicting long-term loads for ultimate limit states. Table 3 shows that skewness, kurtosis and peak factor estimates from the simulations are always larger with nonlinear waves. As a result, extreme loads predicted based on the use of nonlinear waves will also be larger. Furthermore, increments in skewness, kurtosis and peak factor (or deviations from the Gaussian) due to nonlinear, and non-Gaussian, waves are larger for the base shear than for the bending moment; this, again, is because waves affect base shear more directly.

We study a representative 200-second segment from a single ten-minute simulation time history to further understand the influence of wave nonlinearity. Figure 4a shows that crests of the sea surface elevation process, and those of fore-aft tower bending moment and base shear, are systematically higher for the nonlinear wave model than for the linear model. Moreover, the maxima of tower loads occur almost at same instant as the maxima of sea surface elevation, which clearly indicates that the maxima of tower loads is influenced by waves. In a previous study,[34] correlations of occurrences of large loads and large wave heights have been used to show that the influence of the nonlinear wave model on extreme loads becomes more pronounced at larger wave heights.

The power spectrum of the sea surface elevation (Fig. 4b) for the nonlinear case shows a secondary peak at about 0.16 Hz, which is twice the spectral peak frequency of 0.08 Hz (since T_p = 12.3 sec), and another small peak close to a zero frequency. Such secondary peaks arise due to sum and difference interactions of frequencies according to the second-order nonlinear wave model (see Eq. 3). These secondary peaks also appear in power spectra of both the tower base shear and the tower bending moment (Fig. 4b). The tower bending moment power spectrum has a significant peak at around 0.27 Hz, which is the natural frequency for the first bending mode of vibration of the tower in the fore-aft direction; the peak is somewhat suppressed but that is due to the aerodynamic damping from turbine rotor.[31,35,36] These observations suggest that tower dynamics, which may be important in the overall response, may be influenced by the nonlinear waves.

Using the statistics, time-series and power spectral density of load process, we have shown that the nonlinear waves, which better represent waves in the shallow water depths, can influence the tower loads. We next discuss how nonlinear waves affect long-term tower loads, which are relevant in the design of offshore wind turbines.

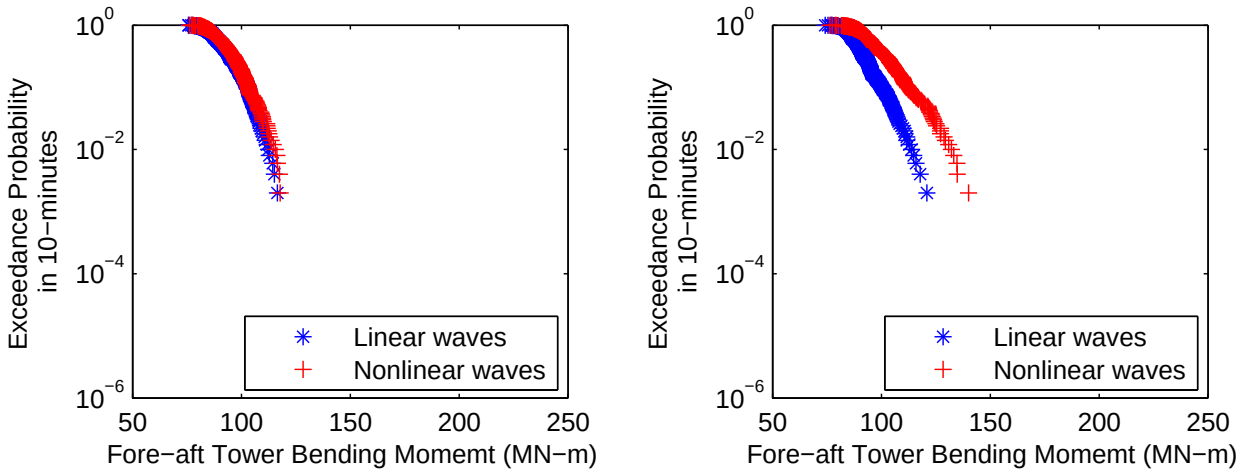

(a) $V = 16$ m/s, $H_s = 5.5$ m. (b) $V = 18$ m/s, $H_s = 7.5$ m.

Figure 5. Empirical probability distributions of ten-minute maxima of the fore-aft tower bending moment at the mudline based on 500 ten-minute simulations.

IV.C. Long-term Loads

In the design of offshore (as well as onshore) wind turbines, one is required to compute long-term loads for a return period on the order of 20 or 50 years. Such long-term loads, according to the design standard[4] from International Electrotechnical Commission (IEC), are to be computed using the statistical extrapolation method. The load extremes data required for the statistical extrapolation in obtained by stochastic turbine response simulations in time domain. While we have so far discussed how nonlinear waves influence the turbine response for a given environmental state, we now discuss how long-term loads differ when irregular waves are modeled using linear or nonlinear theory. We would like to note that the effect of the alternative wave models on long-term turbine loads was discussed in detail in a previous study[34] by authors, and we briefly present a few results here to highlight why it is important to incorporate the nonlinear irregular waves in the coupled simulation of offshore wind turbines, which is the focus of this paper.

In the statistical extrapolation using the so-called direct integration method, one estimates the turbine nominal load for design, l_T, associated with an acceptable probability of exceedance, P_T, or, equivalently, with a target return period of T years, as follows:

$$P_T = P\left[L > l_T\right] = \int_{\boldsymbol{X}} P\left[L > l_T | \boldsymbol{X} = \boldsymbol{x}\right] f_{\boldsymbol{X}}(\boldsymbol{x}) d\boldsymbol{x} \tag{22}$$

where $f_{\boldsymbol{X}}(\boldsymbol{x})$ represents the joint probability density function of the environmental random variables, $\boldsymbol{X}$, and L represents the load measure of interest. For different trial values of the load, l_T, Eq. 22 enables one to compute the long-term probability by integrating the short-term load exceedance probability conditional on $\boldsymbol{X}$, i.e., $P\left[L > l_T | \boldsymbol{X} = \boldsymbol{x}\right]$, with the relative likelihood of different values of $\boldsymbol{X}$. This method, while exact, is expensive as one is required to integrate over the entire domain of all the environmental random variables. In this study, two environmental random variables comprise $\boldsymbol{X}$; these are the ten-minute average wind speed, V, at hub height in the along-wind direction and the significant wave height, H_s, for waves assumed to be aligned with the wind.

The direct integration method is numerically very expensive. An alternative to compute long-term loads is the inverse first-order reliability method (FORM)[37] (see Appendix), which has been shown in an earlier study[38] to be as accurate as the direct integration method for the same offshore wind turbine. The long-term loads discussed in the following have been derived using the inverse FORM. The focus here is how the short-term load distributions, which are required in both the inverse FORM and the direct integration method, are affected when linear or nonlinear irregular waves are used.

Figure 5 shows empirical short-term probability distributions of ten-minute load (fore-aft tower bending moment at the mudline) for the two environmental states: (a) $V = 16$ m/s and $H_s = 5.5$ m, which governed long-term loads when linear waves were used, and (b) $V = 18$ m/s and $H_s = 7.5$ m, which was the governing environmental state for nonlinear waves. The distributions of load maxima for linear and nonlinear waves

Table 4. Extrapolated 20-year long-term loads (10-min maximum fore-aft tower bending moment at mudline) from 50 simulations.

		Ten-minute maximum fore-aft tower bending moment at mudline		
V	H_s	wave model		
(m/s)	(m)	Linear (MN-m)	Nonlinear (MN-m)	ratio -
16	5.5	125.6	128.1	1.02
18	7.5	117.7	138.4	1.18

are quite different for $V = 18$ m/s and $H_s = 7.5$ m while they are almost identical for $V = 16$ m/s and $H_s = 5.5$ m, which shows that nonlinear waves have a greater influence on extreme loads for larger significant wave heights.

Table 4 shows extrapolated 20-year loads estimated using the inverse FORM. Listed are the median estimates of long-term loads obtained from ten sets of 50 simulations. To estimate the desired fractile level corresponding to the return period of 20 years, a two-parameter Weibull distribution was fitted to the above-median (i.e., the largest 25 load extremes out of 50) load extremes. The required exceedance probabilities (estimated using Eq. 32) are 2.03×10^{-3} and 3.87×10^{-6} for $V = 18$ m/s, $H_s = 7.5$ m and $V = 16$ m/s, $H_s = 5.5$ m, respectively. For $V = 18$ m/s, $H_s = 7.5$ m, the extrapolated load change from 118 MN-m for linear waves to 138 MN-m for nonlinear waves, an increase of about 18%. Clearly, long-term loads can be unconservative if linear waves are used.

V. Summary and Conclusions

We incorporated a second-order nonlinear wave model in the coupled aero-servo-hydro-elastic simulation of offshore wind turbines in time domain. The objective was to have an irregular wave model that is more appropriate for shallow water depths, where most offshore wind turbines are sited, than the commonly used linear irregular wave model. We presented the theoretical formulation for the second-order nonlinear irregular waves as developed by Sharma and Dean.[9] We outlined an efficient algorithm for numerical simulation of sea surface elevation and water particle kinematics for irregular nonlinear waves.

We investigated the effect of linear versus nonlinear irregular wave models on the response and the long-term loads for a utility-scale 5MW offshore wind turbine sited in 20 meters of water. This turbine has a monopile support structure (a cylinder of 6 m diameter). Our focus was primarily on the fore-aft tower bending moment at the mudline. Using a representative environmental state, we showed that the nonlinear waves result in larger loads than those due to linear waves. The loads due to nonlinear waves tend to be more non-Gaussian and, therefore, extreme loads due to nonlinear waves are predicted to be larger. Moreover, nonlinear waves also influence the dynamic behavior of the tower loads.

Finally, we studied the influence of the alternate irregular wave models on the short-term load distributions, and on the long-term loads, which are of interest in the design of turbines, for a return period of 20 years. It was found that the loads associated with rare fractile levels in short-term distributions and the long-term loads can be significantly higher when nonlinear waves. In other words, estimated long-term loads can be unconservative if the simplistic linear irregular wave model is used.

VI. Appendix

VI.A. Transfer Functions for Second-Order Irregular Waves

The transfer functions B^-_{mn} and B^+_{mn} in Eq. 3 are given by:

$$B^-_{mn} = \frac{1}{4}\left[\frac{D^-_{mn} - (k_m k_n + R_m R_n)}{\sqrt{R_m R_n}} + (R_m + R_n)\right] \tag{23}$$

$$B^{+}_{mn} = \frac{1}{4}\left[\frac{D^{+}_{mn} - (k_m k_n - R_m R_n)}{\sqrt{R_m R_n}} + (R_m + R_n)\right] \tag{24}$$

where

$$D^{-}_{mn} = \frac{(\sqrt{R_m} - \sqrt{R_n})\left\{\sqrt{R_n}(k_m^2 - R_m^2) - \sqrt{R_m}(k_n^2 - R_n^2)\right\}}{(\sqrt{R_m} - \sqrt{R_n})^2 - k^{-}_{mn}\tanh(k^{-}_{mn}h)} + \frac{2(\sqrt{R_m} - \sqrt{R_n})^2(k_m k_n + R_m R_n)}{(\sqrt{R_m} - \sqrt{R_n})^2 - k^{-}_{mn}\tanh(k^{-}_{mn}h)} \tag{25}$$

$$D^{+}_{mn} = \frac{(\sqrt{R_m} + \sqrt{R_n})\left\{\sqrt{R_n}(k_m^2 - R_m^2) + \sqrt{R_m}(k_n^2 - R_n^2)\right\}}{(\sqrt{R_m} + \sqrt{R_n})^2 - k^{+}_{mn}\tanh(k^{+}_{mn}h)} + \frac{2(\sqrt{R_m} + \sqrt{R_n})^2(k_m k_n - R_m R_n)}{(\sqrt{R_m} + \sqrt{R_n})^2 - k^{+}_{mn}\tanh(k^{+}_{mn}h)} \tag{26}$$

In the above, k is the wave number which is related the frequency, ω, and the water depth, h, via the dispersion relation. Related parameters that are needed are given as follows:

$$\omega^2 = gk\tanh(kh) \tag{27}$$

$$R_m = \frac{\omega_m^2}{g} \tag{28}$$

$$k^{-}_{mn} = |k_m - k_n| \tag{29}$$

$$k^{+}_{mn} = k_m + k_n \tag{30}$$

where g refers to acceleration due to gravity.

VI.B. Inverse First-order Reliability Method

In the inverse FORM, for the present application, one considers a surface in a three-dimensional space, $\boldsymbol{Y} = (V, H_s, L)$, of physical random variables, on one side of which (i.e., the "failure" side), it is assumed that $L > l_T$. It is possible to mathematically transform this space to an independent standard normal space $\boldsymbol{U} = (U_1, U_2, U_3)$. A sphere of radius, β, in the standard normal space is defined as follows:

$$u_1^2 + u_2^2 + u_3^2 = \beta^2 \tag{31}$$

This sphere is such that all values of $\boldsymbol{U}$ within it occur with a probability greater than P_T while all values outside it occurs with a probability less than P_T.

It is noted here that β is directly related to the target probability of load exceedance; namely, $P_T = \Phi(-\beta)$, where $\Phi()$ represents the cumulative distribution function of a standard normal random variable. The transformation of the random variables involved from the physical space, $\boldsymbol{Y}$, to the standard normal $\boldsymbol{U}$ space is carried out via the Rosenblatt transformation such that $F_V(v) = \Phi(u_1)$, $F_{H|V}(h) = \Phi(u_2)$, and $F_{L|V,H}(l) = \Phi(u_3)$, where $F()$ denotes the cumulative distribution function in each case. A point on the sphere defined by Eq. 31 where the load attains its maximum value is the "design" point, and this load represents the desired nominal T-year return period load, l_T.

According to inverse FORM, we estimate the load for the fractile level, $p_3 = \Phi(u_3)$, for all possible (V, H_s) pairs, and largest of such load fractiles is the nominal load, l_T. Based on Eq. 31, the fractile level, p_3, corresponding to the target reliability index, β, is obtained as follows:

$$p_3 = \Phi\left(\sqrt{\beta^2 - \left[\Phi^{-1}\left(F_V(v)\right)\right]^2 - \left[\Phi^{-1}\left(F_{H|V}(h)\right)\right]^2}\right) \tag{32}$$

VII. Acknowledgments

The authors gratefully acknowledge assistance received with the 5MW offshore wind turbine baseline model used in the simulation studies from Dr. Jason Jonkman of the National Renewable Energy Laboratory.

The authors also wish to acknowledge the financial support provided by the National Science Foundation (CAREER Award No. CMMI-0449128 and Award No. CMMI-0727989) and by Sandia National Laboratories (Contract No. 743358). The first author also acknowledges Stress Engineering Services for providing financial support to attend the conference.

References

[1]Musial, W. and Butterfield, S., "Future for Offshore Wind Energy in the United States," Tech. Rep. NREL/CP-500-36313, National Renewable Energy Laboratory, Golden, CO, 2004.

[2]European Wind Energy Association, *Response to the European Commissions's Green Paper: A European Strategy for Sustainable, Competitive and Secure Energy, EWEA Position Paper*, Brussels, Belgium, 2006.

[3]European Wind Energy Association, *Delivering Offshore Wind Power in Europe — Policy Recommendations for Large-scale Deployment of Offshore Wind Power in Europe by 2020*, Brussels, Belgium, 2007.

[4]IEC-61400-3, *Wind Turbines - Part 3: Design Requirements for Offshore Wind Turbines*, International Electrotechnical Commission, TC88 WG3 Committee Draft, 2005.

[5]DNV-RP-C205, *Environmental Conditions and Environmental Loads, Recommended Practice*, Det Norske Veritas, 2007.

[6]Forristall, G. Z., "Nonlinear Wave Calculations for Engineering Applications," *Journal of Offshore Mechanics and Arctic Engineering*, Vol. 124, No. 1, 2002, pp. 28–33.

[7]Jha, A. K., *Nonlinear Stochastic Models for Ocean Wave Loads and Responses of Offshore Structures and Vessels*, Ph.D. Dissertation, Stanford University, 1997.

[8]ITTC, "The Specialist Committee on Environmental Modeliing, Final Report and Recommendations to the 22nd ITTC," Tech. rep., International Towing Tank Conference, Seoul, 1999.

[9]Sharma, J. N. and Dean, R. G., "Development and Evaluation of a Procedure for Simulating a Random Directional Second-order Sea Surface and Associated Wave Forces," Tech. Rep. Ocean Engineering Report No. 20, University of Delaware, Newark, DE, 1979.

[10]Longuet-Higgins, M., "Resonant Interactions between two Trains of Gravity Waves," *Journal of Fluid Mechanics*, Vol. 12, No. 3, 1962, pp. 321–332.

[11]Hasselmann, K., "On the Non-linear Energy Transfer in a Gravity Wave Spectrum, Part 1, General Theory," *Journal of Fluid Mechanics*, Vol. 12, 1962, pp. 481–500.

[12]Hu, S.-L. J. and Zhao, D., "Non-Gaussian Properties of Second-order Random Waves," *Journal of Engineering Mechanics*, Vol. 119, No. 2, 1993, pp. 344–364.

[13]Langley, R., "A Statistical Analysis of Nonlinear Random Waves," *Ocean Engineering*, Vol. 14, No. 5, 1987, pp. 389–407.

[14]Longuet-Higgins, M., "The Propagation of Short Surface Waves on Longer Gravity Waves," *Journal of Fluid Mechanics*, Vol. 177, 1987, pp. 293–306.

[15]Forristall, G. Z., "Wave Crest Distributions: Observations and Second-Order Theory," *Journal of Physical Oceanography*, Vol. 30, No. 8, 2000, pp. 1931–1943.

[16]Forristall, G. Z., "Irregular Wave Kinematics from a Kinematic Boundary Condition Fit (KBCF)," *Applied Ocean Research*, Vol. 7, No. 4, 1985, pp. 202–212.

[17]Tromans, P. S., Anaturk, A. R., and Hagemeijer, P., "A New Model for Kinematics of Large Ocean Waves — Application as a Design Wave," *1st International Offshore and Polar Engineering Conference, ISOPE1991*, Vol. 3, Edinburg, Scotland, 1991.

[18]Taylor, P. H., Jonathan, P., and Harland, L. A., "Time-domain Simulation of Jack-up Dynamics with the Extremes of a Gaussian Process," *14th International Conference on Offshore Mechanics and Arctic Engineering, OMAE1995*, Volume 1A, pp. 313-319, Copenhagen, Denmark, 1995, pp. 313–319.

[19]Zhang, J., Chen, L., Ye, M., and Randall, R. E., "Hybrid Wave Model for Unidirectional Irregular Waves — Part I. Theory and Numerical Scheme," *Applied Ocean Research*, Vol. 18, 1996, pp. 77–92.

[20]Nwogu, O., "Alternative form of Boussinesq Equations for Nearshore Wave Propagation," *Journal of Waterway, Port, Coastal and Ocean Engineering*, Vol. 119, No. 6, 1993, pp. 618–638.

[21]Madsen, P. A., Bingham, H. B., and Liu, H., "A new Boussinesq method for Fully Nonlinear Waves from Shallow to Deep Water," *Journal of Fluid Mechanics*, Vol. 462, 2002, pp. 1–30.

[22]Jonkman, J. M. and Buhl Jr., M. L., "FAST User's Guide," Tech. Rep. NREL/EL-500-38230, National Renewable Energy Laboratory, Golden, CO, 2005.

[23]Jonkman, J. M., Butterfield, S., Musial, W., and Scott, G., "Definition of a 5-MW Reference Wind Turbine for Offshore System Development," Tech. Rep. NREL/TP-500-38060, National Renewable Energy Laboratory, Golden, CO, 2007 (to be published).

[24]Burton, T., Sharpe, D., Jenkins, N., and Bossanyi, E., *Wind Energy Handbook*, John Wiley, Chichester, England, 2001.

[25]Barltrop, N. D. P. and Adams, A. J., *Dynamics of Fixed Marine Structures*, Third Edition, Butterworth-Heinemann, London, 1991.

[26]Sarpkaya, T. and Issacson, M., *Mechanics of Wave Forces on offshore Structures*, Van Nostrand Reinhold, New York, 1981.

[27]Sharma, J. N., *Development and Evaluation of a Procedure for Simulating a Random Directional Second-order Sea Surface and Associated Wave Forces*, Ph.D. thesis, University of Delaware, Delaware, 1979.

[28]Hudspeth, R. and Chen, M.-C., "Digital Simulation of Nonlinear Random Waves," *Journal of Waterway, Port, Coastal and Ocean Division, ASCE*, Vol. 105, No. WW1, 1979, pp. 67–85.

[29]Hu, S.-L. J., *Nonlinear Random Water Wave*, In Computational Stochastic Mechanics, A.H.-D. Chang and C.Y.Yang, eds., Computational Mechanics Publication, Southampton, UK, 519-544, 1993.

[30]Shinozuka, M. and Deodatis, G., "Simulation of Stochastic Processes by Spectral Representation," *Applied Mechanics Reviews*, Vol. 44, No. 4, 1991, pp. 191–203.

[31]Agarwal, P. and Manuel, L., "Wave Models for Offshore Wind Turbines," *ASME Wind Energy Symposium, AIAA*, Reno, NV, 2008.

[32]Jonkman, B. J. and Buhl Jr., M. L., "TurbSim User's Guide," Tech. Rep. NREL/TP-500-41136, National Renewable Energy Laboratory, Golden, CO, 2007.

[33]DNV-OS-J101, *Design of Offshore Wind Turbine Structures, Offshore Standard*, Det Norske Veritas, 2007.

[34]Agarwal, P. and Manuel, L., "Modeling Nonlinear Irregular Waves in Reliability Studies for Offshore Wind Turbines," *28th International Conference on Offshore Mechanics and Arctic Engineering, OMAE2009*, Paper no. 80149, Honolulu, Hawai, 2009.

[35]Jonkman, J., Butterfield, S. P., Passon, P., Larsen, T., Camp, T., Nichols, J., Azcona, J., and Martinez, A., "Offshore Code Comparison Collaboration within IEA Wind Annex XXIII: Phase II Results Regarding Monopile Foundation Modeling," Tech. Rep. NREL/CP-500-42471, National Renewable Energy Laboratory, Golden, CO, 2008.

[36]Tempel, J. and Molenaar, D.-P., "Wind Turbine Structural Dynamics - A Review of the Principles for Modern Power Generation, Onshore and Offshore," *Wind Engineering*, Vol. 26, No. 4, 2002, pp. 211–220.

[37]Winterstein, S. R., Ude, T. C., Cornell, C. A., Bjerager, P., and Haver, S., "Environmental Contours for Extreme Response: Inverse FORM with Omission Factors," *Proceedings, ICOSSAR-93*, Innsbruck, Austria, 1993.

[38]Agarwal, P. and Manuel, L., "Simulation of Offshore Wind Turbine Response for Extreme Limit States," *26th International Conference on Offshore Mechanics and Arctic Engineering, OMAE2007*, Paper no. 29326, San Diego, CA, 2007.